Dalton Transactions

ROYAL SOCIETY OF CHEMISTRY

PAPER

View Article Online
View Journal | View Issue

Cite this: *Dalton Trans.*, 2023, **52**, 10844

Atomic layer deposition of CoF_2, NiF_2 and HoF_3 thin films

Elisa Atosuo, *[a] Miia Mäntymäki, [a] Leevi Pesonen,[a] Kenichiro Mizohata,[b] Timo Hatanpää, [a] Markku Leskelä [a] and Mikko Ritala *[a]

The present study describes atomic layer deposition (ALD) processes and characterization of CoF_2, NiF_2, and HoF_3 thin films. For CoF_2 deposition $CoCl_2$(TMEDA) (TMEDA = *N*,*N*,*N*′,*N*′-tetramethylethylenediamine) and NH_4F were used as precursors. CoF_2 deposition was studied at 180–275 °C, resulting in a growth per cycle (GPC) of 0.7 to 1.2 Å. All the films consist of tetragonal CoF_2 according to XRD. The impurity contents were measured with ToF-ERDA and less than 1 at% of N and Cl were detected in the films, indicating effective reactions. In addition, the F/Co ratio is close to 2 as measured by the same method. The saturation of the GPC with respect to precursor pulses and purges was verified at 250 °C. The common feature of ALD metal fluoride films – remarkable roughness – is encountered also in this process. However, the films became smoother as the deposition temperature was increased. CoF_2 deposition was also demonstrated on graphite substrates. NiF_2 deposition was studied at 210–250 °C by using $Ni(thd)_2$ and TaF_5 or a new fluoride source NbF_5 as the precursors. Tetragonal NiF_2 was obtained, but the oxygen and hydrogen contents in the films were remarkable, up to ~11 at%, as measured by ToF-ERDA. This was observed also when the films were *in situ* capped with YF_3. NbF_5 was shown to be a potential fluoride precursor by combining it with $Ho(thd)_3$ to deposit HoF_3 films. Orthorhombic HoF_3 was obtained at deposition temperatures of 200–275 °C. The films deposited at 235–275 °C are pure, and the Nb contents in films deposited at 250 and 275 °C are only 0.21 and 0.15 at%. The main impurity in both films is oxygen, but the contents are only 1.5 and 1.6 at%. The saturation of the GPC with respect to precursor pulses was verified at 250 °C. The GPC is ~1 Å.

Received 4th June 2023,
Accepted 18th July 2023

DOI: 10.1039/d3dt01717f

rsc.li/dalton

Introduction

Lithium-ion batteries (LIBs) have been considered as the best choice for challenging energy storage, such as transport, due to their good gravimetric and volumetric energy densities, long cycle life and relatively low cost. To make the most of the LIB technology, research is now focusing on, *e.g.*, 3D solid-state batteries. The performance of 3D solid-state batteries can be improved by developing new cathode materials which have higher capacities than the currently used intercalation transition metal oxides.

One of the active cathode research topics has been transition metal fluorides. They are potential cathode materials for both Li and Na-based battery systems and surpass the commonly used metal oxides in energy densities. The operation principle of transition metal fluoride cathodes is based on conversion reactions with lithium ions. Compared to the conventional layered intercalation oxide cathodes, transition metal fluorides can provide higher capacities due to more transferring electrons per one transition metal ion. In addition, the conversion reactions go to completion, as opposite to the intercalation reactions in the layered oxides, where typically only a fraction of the redox-active metals can be utilized. A selection of conversion cathode materials, such as FeF_2, FeF_3, CoF_2, CoF_3, NiF_2, and CuF_2 have been studied.[1]

For the future 3D solid-state batteries, cathode materials are needed in the form of conformal thin films. However, not many methods have been reported for fabricating thin films of the discussed metal fluorides. For cobalt(II) fluoride, for example, only pulsed laser deposition (PLD), thermal evaporation and molecular beam epitaxy (MBE) have been reported.[2–6] To realize complicated structures needed for 3D solid-state batteries, a sophisticated thin film manufacturing method, such as atomic layer deposition (ALD), is needed. ALD is an advanced version of chemical vapor deposition (CVD) technique. The characteristics of ALD are its ability to uniformly coat 3D shapes, easily controllable film thickness, excellent film purity and stoichiometry, reproducibility, and in general lower deposition temperatures compared to the traditional CVD. These features arise from the self-limiting reactions of the gaseous precursors.[7]

[a]*Department of Chemistry, University of Helsinki, Finland.*
E-mail: elisa.atosuo@helsinki.fi
[b]*Department of Physics, University of Helsinki, Finland*

Thanks to the advantageous nature of ALD, many battery component materials (electrodes, solid electrolytes, barrier layers, and artificial electrode–electrolyte interface layers) have already been deposited with ALD.[8] These processes include also some metal fluorides, *e.g.*, LiF and AlF_3 which can serve as protective layers for the electrodes.[9,10] Common to all the above-listed metal fluoride cathode materials FeF_2, FeF_3, CoF_2, CoF_3, NiF_2, and CuF_2 is that they lack an ALD process.

In this work, an ALD process for CoF_2 is reported. CoF_2 was deposited by using $CoCl_2$(TMEDA) (TMEDA = *N*,*N*,*N*′,*N*′-tetramethylethylenediamine) and NH_4F as precursors. Also deposition of NiF_2 was attempted. However, NiF_2 deposition was not straightforward with traditional precursor combinations, and film growth was observed only with the combination of Ni(thd)$_2$ (thd = 2,2,6,6-tetramethyl-3,5-heptanedionato) and TaF_5 or NbF_5. In addition, the hygroscopicity of NiF_2 was noticed to cause remarkable issues to the deposition process. Since NbF_5 was however identified as a potential fluoride source, we studied its usability in ALD by studying the deposition of a more stable metal fluoride, holmium fluoride. NbF_5 was combined with Ho(thd)$_3$ to produce HoF_3 films.

Experimental section

Film deposition

The films were deposited in an F120 cross-flow reactor (ASM Microchemistry Ltd) using 99.999% nitrogen as carrier and purging gas. In-house synthesized $CoCl_2$(TMEDA) and Co(thd)$_2$ (Volatec Oy) were used as cobalt precursors. Their sublimation temperatures were 170 and 98–110 °C. The synthesis of the $CoCl_2$(TMEDA) precursor is presented elsewhere.[11] NiF_2 film deposition was studied by using Ni(thd)$_2$ (Volatec Oy) and in-house synthesized $NiCl_2$(TMPDA) as nickel precursors. The evaporation temperatures were 125 °C for Ni(thd)$_2$ and 157 °C for $NiCl_2$(TMPDA). The synthesis of the $NiCl_2$(TMPDA) precursor is presented elsewhere.[12] HoF_3 films were deposited with Ho(thd)$_3$ (Volatec Oy) as the holmium precursor. The evaporation temperature was 125 °C.

NH_4F (Sigma-Aldrich, ≥99.99%), TiF_4 (Strem, 98%), TaF_5 (Alfa Aesar, 99.9%) and NbF_5 (abcr GmbH, 99.5%) were used as fluoride precursors. Their sublimation temperatures were 65–67, 135–145, 45 and 40–45 °C, respectively.

The films were mainly deposited on Si(100) substrates with the native oxide. CoF_2 deposition was studied also on graphite substrates (99.95% carbon foil from Goodfellow). The films were stored in a desiccator after deposition.

Film characterization

Thicknesses of the films were measured with a Film Sense FS-1 multiwavelength ellipsometer by fitting the data with a Cauchy model. Also energy dispersive X-ray spectroscopy (EDS) was used for the thickness determination using an Oxford INCA 350 microanalysis system connected to a Hitachi S-4800 field-emission scanning electron microscope (FESEM). The thicknesses were calculated with the GMRFILM program. Some film thicknesses were confirmed with cross-section FESEM.

EDS was used also to confirm the elements present in the films. Prior to the EDS measurements, the films were coated with carbon to increase the conductivity of the films.

Time-of-flight recoil detection analysis (ToF-ERDA) was used to quantitatively determine the stoichiometry of the films and the impurity contents. A 5 MV tandem accelerator at the accelerator laboratory of University of Helsinki was used for measurements. Measurements were done using 35–40 MeV ^{79}Br or ^{127}I primary ions and 40° detection angle.

PANalytical X′pert Pro MPD diffractometer in the grazing incidence X-ray diffraction mode (GI-XRD) was used for crystallinity measurements. The diffractograms were analyzed with a PANalytical HighScore plus software (version 4.7).

FESEM and atomic force microscopy (AFM) were used for studying the morphology of the films. A Veeco Multimode V instrument was used for recording the AFM images. Tapping mode images were captured in air using silicon probes with nominal tip radius of 10 nm and nominal spring constant of 5 N m^{-1} (Tap150 from Bruker). Images were flattened to remove artefacts caused by sample tilt and scanner bow. Roughness was calculated as a root-mean-square value (R_q). For FESEM imaging, the films were coated with Au/Pd to increase the conductivity of the samples.

Thermodynamic calculations were done with HSC Chemistry 7.1 software (Outokumpu Research Oy).

Results and discussion

Cobalt(II) fluoride films

CoF_2 deposition was attempted with the combinations of Co(thd)$_2$ (thd = 2,2,6,6-tetramethyl-3,5-heptanedionato) and NH_4F, TiF_4, TaF_5, or NbF_5. With NH_4F no film was obtained. With TiF_4 the film deposited at 200 °C possibly consisted of CoF_2 according to XRD, but for the film deposited at 300 °C XRD showed strongly crystalline TiF_3 phase in addition to the possible CoF_2 phase. The combinations of Co(thd)$_2$ and TaF_5 or NbF_5 were briefly studied at the deposition temperature of 250 °C. In both cases CoF_2 phase was seen in XRD. However, in the case of NbF_5 the film was blurry and contained ~5 at% of Nb according to EDS. In the case of TaF_5 the film contained more tantalum than cobalt according to EDS.

CoF_2 was successfully deposited by using $CoCl_2$(TMEDA) (TMEDA = *N*,*N*,*N*′,*N*′-tetramethylethylenediamine) and NH_4F as precursors. $CoCl_2$(TMEDA) is a volatile adduct of the extremely low-volatility $CoCl_2$. It was first presented by Väyrynen *et al.* in an ALD process for cobalt(II) oxide.[11] The neutral adduct ligand TMEDA is assumed to be released during the chemisorption of the molecule on the growth surface. NH_4F in turn decomposes to HF and NH_3 inside the ALD reactor upon heating.[13]

The evaporation temperature of $CoCl_2$(TMEDA) is 170 °C and it has been reported to decompose at 300 °C.[11] The deposition was thus studied at temperatures of 180–300 °C. After

confirming that the precursor combination produces CoF_2 films, the saturation of the growth per cycle (GPC) was studied at 250 °C using 1000 cycles. The NH_4F pulse was studied first by keeping the $CoCl_2$(TMEDA) pulses and purges at 1 s. Soft saturation was observed when 3 s NH_4F pulses were applied (Fig. 1a, black squares). The effect of the $CoCl_2$(TMEDA) pulses was studied by keeping the NH_4F pulses at 3 s and the purges at 1 s. For $CoCl_2$(TMEDA) 0.5 s pulses were sufficient to reach saturation (Fig. 1b). Later, however, it was noticed that more uniform films were obtained when the evaporation temperature of NH_4F was increased by a couple of degrees to 67 °C. The saturation of the GPC was studied again by using 1 s $CoCl_2$(TMEDA) pulses and 4 s purges (Fig. 1a, red triangles). A better saturation curve was achieved, and 3 s NH_4F pulses were sufficient for the saturation. It was also verified that 3 s purges are sufficient (Fig. 1a, blue circle). The GPC is 1.15 Å.

CoF_2 films were deposited at 250 °C also with 250, 500, and 1500 cycles to study the linearity of the growth. As seen in Fig. 2, the thickness of the films grows linearly with the increasing cycle number.

Film growth was studied at 180–300 °C. The lowest deposition temperature 180 °C is only 10 °C higher than the evaporation temperature of the metal precursor but results in uniform films. At 300 °C, in turn, very spotty films were obtained, and this temperature was not studied further. The adhesion of the films to the Si substrate was in general good as was tested with the Scotch tape test.

Fig. 3 shows the GPC of the films deposited at different temperatures using 1000 cycles as calculated from ellipsometry and EDS. In general, the EDS and ellipsometry results are in line with each other at high deposition temperatures, whereas at lower temperatures the difference is larger. This might be explained by the large roughness of the films deposited at lower temperatures which complicates the ellipsometry measurements. Nevertheless, as seen in the EDS results, the trend in the GPC is increasing from 180 to 225 °C and the GPC stays approximately constant at 225 and 250 °C. The GPC increases again at 275 °C. The increase could be explained by the onset of the precursor decomposition as $CoCl_2$(TMEDA) has been reported to decompose at 300 °C and above.

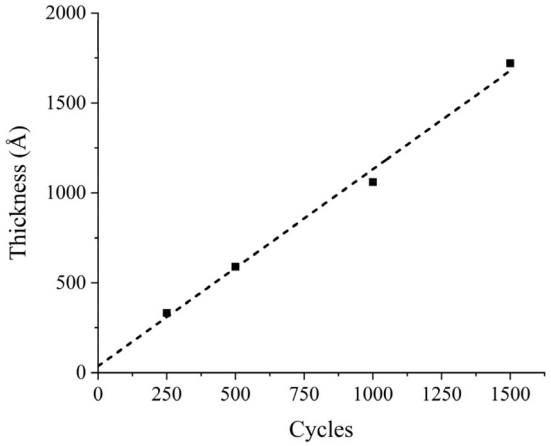

Fig. 2 Thickness of the films as a function of CoF_2 deposition cycles.

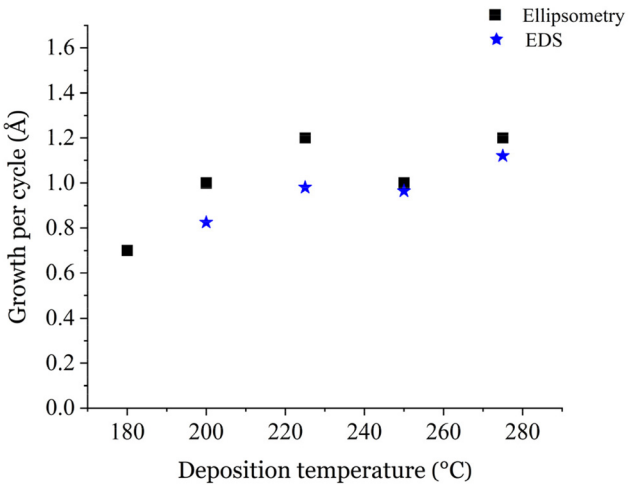

Fig. 3 GPC of CoF_2 films as a function of the deposition temperature.

All the deposition temperatures (180–300 °C) result in polycrystalline tetragonal CoF_2 films as measured by XRD (Fig. 4, ICDD PDF 33-417). There are however differences in the relative diffraction intensities of films deposited at different temp-

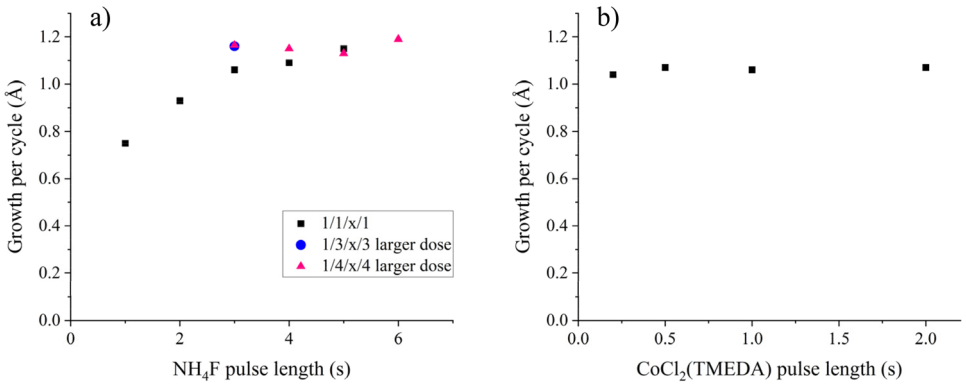

Fig. 1 GPC as a function of (a) NH_4F and (b) $CoCl_2$(TMEDA) pulse lengths at 250 °C.

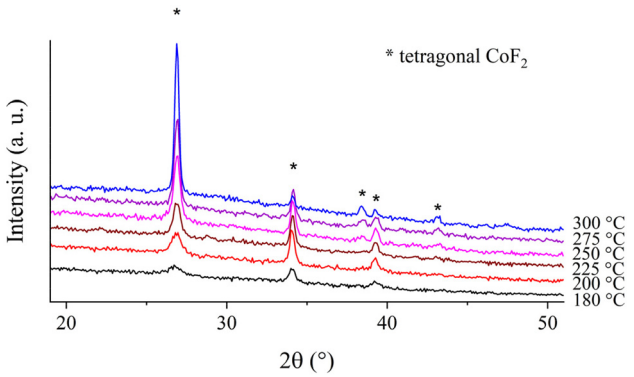

Fig. 4 GI-XRD of CoF_2 films deposited at 180–300 °C. The films are 60–69 nm thick, except the film deposited at 180 °C that is 48 nm thick.

eratures which might indicate different orientations. For a randomly oriented CoF_2, the strongest reflection is positioned at 2θ of ~27°. This reflection is seen in our films, and it becomes dominant as the deposition temperature increases. In Fig. 4, the thicknesses of the films are 60–69 nm, except the film deposited at 180 °C which is 48 nm thick. Tetragonal CoF_2 has been obtained also with thermal evaporation method.[5]

The composition of the films was studied qualitatively with EDS. In addition to Co, F, and light impurity elements, a small Ni signal was sometimes observed. The possible explanations for this are nickel residues in the reactor or contaminants in the $CoCl_2$ used for the synthesis of $CoCl_2$(TMEDA).

The impurities as well as the stoichiometry were quantitatively measured with ToF-ERDA. Table 1 represents the elemental contents in the films including the surface and Si/CoF_2 interface regions. The F/Co ratio 1.9–2.2 is close to the expected 2.0 and thus in line with the XRD results. In addition, the impurity contents are low. For example, the N and Cl contents are less than 1 at% in all the measured films, despite both precursors containing nitrogen. The purest films are those deposited at 225–275 °C, having H, C, N, O, and Cl contents lower than 1 at%. At 250 °C, the total content of these impurities is only 1.15 at%. If some precursor decomposition was to take place already at 275 °C, as discussed earlier, it is not seen as increased impurity contents.

The possible nickel contamination cannot be determined with ToF-ERDA because the similar masses of cobalt and nickel makes their separation impossible. However, because Ni was only occasionally detected with EDS, and the small amount of nickel is not assumed to affect the CoF_2 growth, the nickel content was not determined quantitatively with other methods either.

Based on the XRD and ToF-ERDA results, the precursor combination of $CoCl_2$(TMEDA) and NH_4F seems to work well. To our knowledge, no successful ALD process has been reported in the literature using the precursor combination of a metal chloride and NH_4F. These combinations have been previously tested at least for AlF_3 and ZnF_2, but no film growth was observed.[13] It is interesting to note that ZnF_2 films have been deposited by ALD using zinc acetate and NH_4F as precursors.[13] In addition, the $AlCl_3$ + TiF_4 process has been shown to work for AlF_3 deposition.[14]

Fig. 5 shows FESEM images of films deposited at 200, 250, and 275 °C with 1000 cycles. In the film deposited at 200 °C, rod-shaped grains are seen, and the surface appears rough. At 250 and 275 °C, the grains are larger and merged together, making the film appear more uniform and smoother. The difference in the morphology between the films deposited at 200 and 275 °C is seen also in the cross-section FESEM images (Fig. 6).

Also a thinner film (250 cycles) was deposited at 250 °C and imaged with FESEM (Fig. 5). The morphology resembles the film deposited at 200 °C rather than the thicker film deposited at 250 °C. The film is also not yet continuous. The continuity of thin films was not specifically studied, but at least a film deposited with 500 cycles at the same deposition temperature is continuous.

Due to the morphology of the films, their roughness was assumed to be remarkable. Fig. 7 shows AFM images of films deposited at 200–275 °C. Although the films are only 60–69 nm thick, the root mean square roughnesses (R_q) are between 10.9 and 24.7 nm. The largest roughness is measured from the film deposited at the lowest temperature, and the roughness gets smaller as the deposition temperature is increased. This is in line with the FESEM studies. Due to the roughness, the film deposited at the lowest temperature was very difficult to measure with AFM. Note that the z-scales of 200 and 225 °C images are different compared to 250 and 275 °C images.

Since the electronic conductivity of metal fluorides is poor, potential battery materials have been combined, *e.g.*, with carbon to create conducting nanostructures.[15] Therefore, we briefly studied CoF_2 deposition also on a graphite substrate. The deposition was done by applying 700 cycles at 250 °C. The precursor pulse lengths were adopted from the CoF_2 process on Si, but the purge times were lengthened to 5 s. In FESEM images rod-like features are seen (Fig. 8). According to XRD the film consists of tetragonal CoF_2 (Fig. 9).

Table 1 Elemental contents and stoichiometry as measured by ToF-ERDA for CoF_2 films (F/Co ratio 1.9–2.2) deposited with 1000 cycles at different deposition temperatures

T_{dep} (°C)	Co (at%)	F (at%)	H (at%)	C (at%)	N (at%)	O (at%)	Cl (at%)	F/Co
180	33 ± 2	61 ± 5	2.1 ± 0.9	0.62 ± 0.12	0.11 ± 0.01	2.3 ± 0.2	0.60 ± 0.08	1.9
200	31.6 ± 1.0	63 ± 2	3 ± 2	1.1 ± 0.3	0.19 ± 0.08	0.98 ± 0.06	0.28 ± 0.07	2.0
225	32.6 ± 0.8	65 ± 2	0.9 ± 0.3	0.60 ± 0.15	0.04 ± 0.00	0.79 ± 0.06	0.23 ± 0.05	2.0
250	31.2 ± 0.6	68 ± 2	0.25 ± 0.08	0.10 ± 0.01	0.04 ± 0.00	0.63 ± 0.04	0.13 ± 0.02	2.2
275	33.4 ± 0.6	64.1 ± 1.3	0.8 ± 0.3	0.7 ± 0.3	0.03 ± 0.00	0.92 ± 0.06	0.17 ± 0.03	1.9

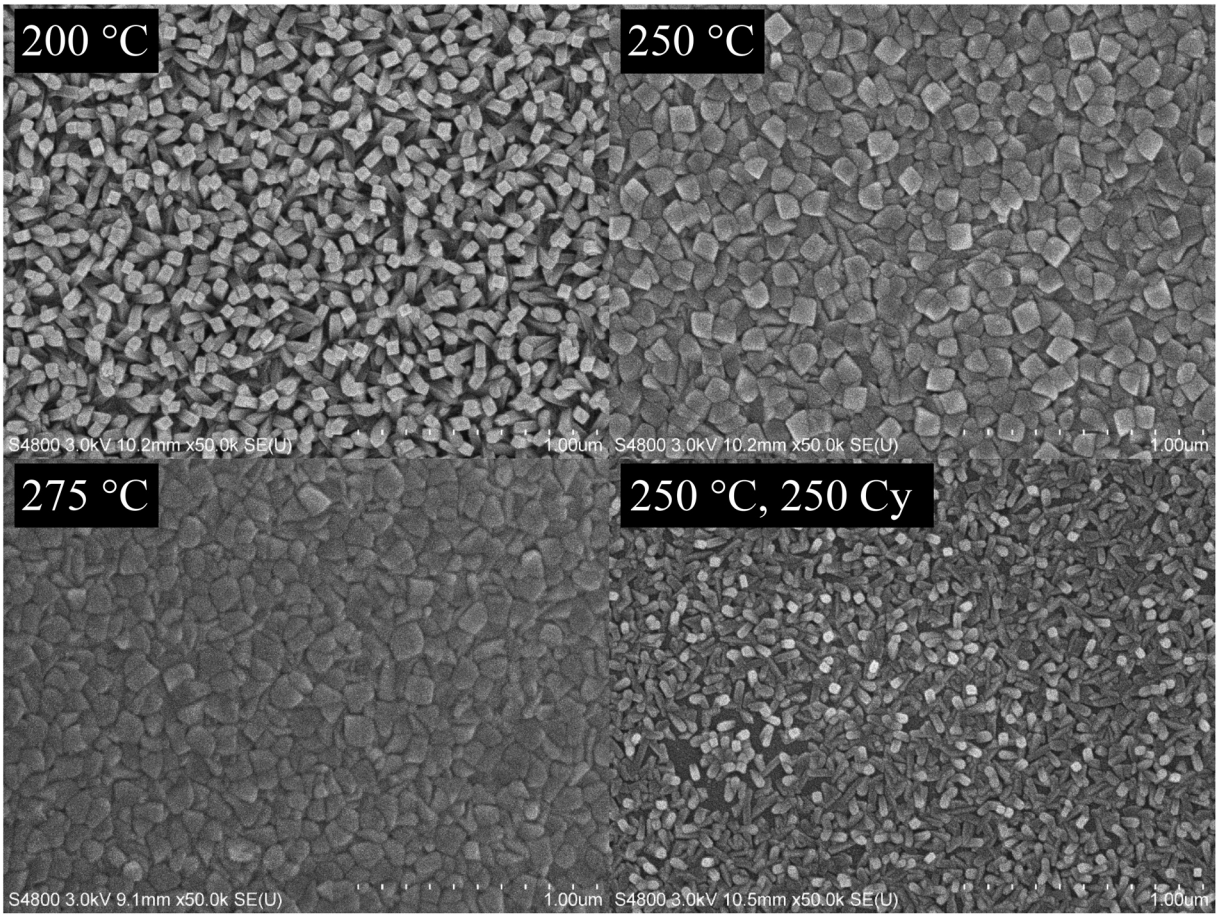

Fig. 5 FESEM images of CoF_2 films deposited at 200, 250, and 275 °C with 1000 cycles and at 250 °C with 250 cycles.

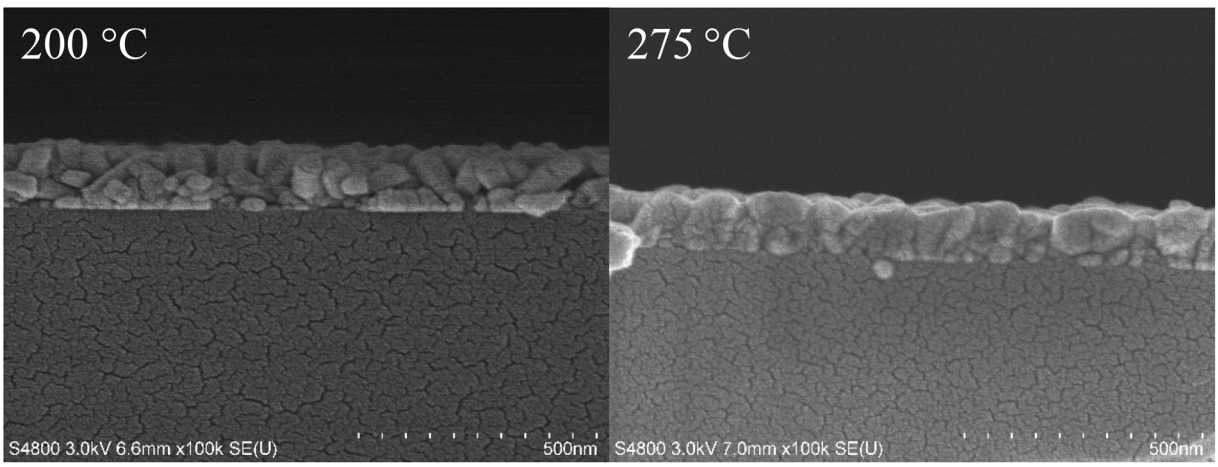

Fig. 6 Cross-section FESEM images of CoF_2 films deposited at 200 and 275 °C with 1000 cycles.

Nickel(II) fluoride films

Nickel(II) fluoride deposition was first attempted with the combination of $NiCl_2$(TMPDA) (TMPDA = *N*,*N*,*N*′,*N*′-tetramethyl-1,3-propanediamine)[12] and NH_4F, which is similar to the precursor combination used in the successful CoF_2 deposition. No film was obtained, however. Also the more traditional precursor combinations of $Ni(thd)_2$ and NH_4F or TiF_4 were studied but no film growth was observed.

NiF_2 growth was achieved with the combination of $Ni(thd)_2$ and NbF_5. The use of NbF_5 as the fluoride source in ALD has been mentioned in patents,[16,17] but to our knowledge no

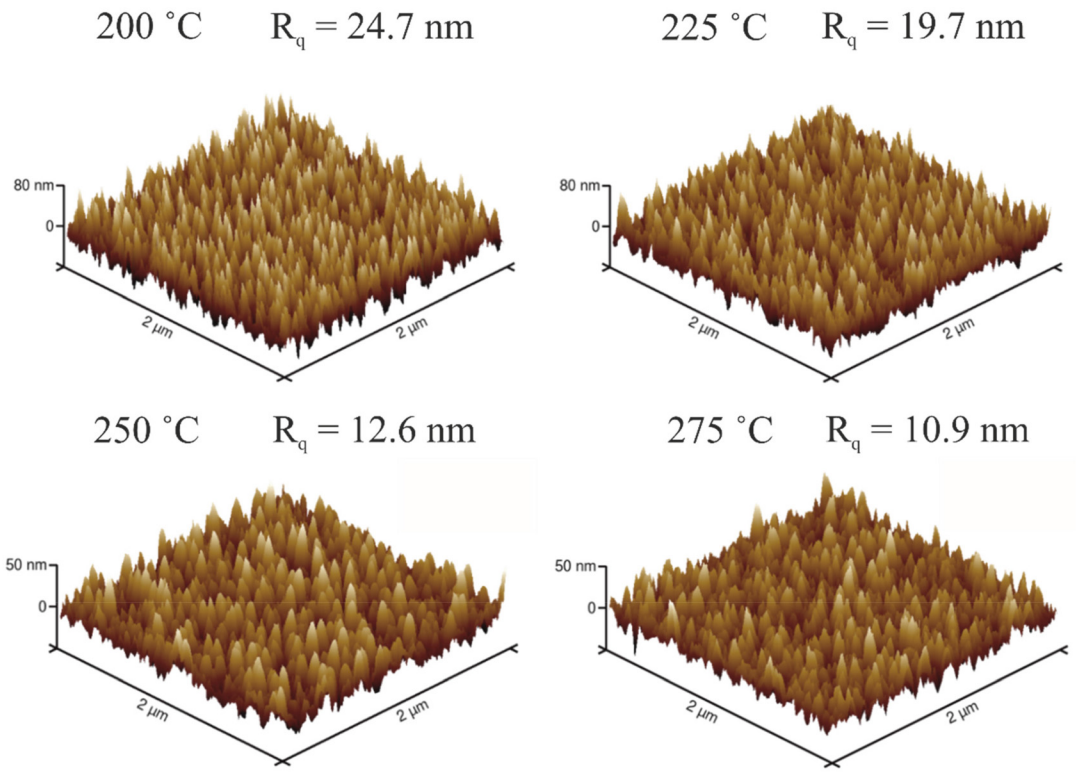

Fig. 7 AFM images of CoF_2 films deposited at 200–275 °C. Note the larger z-scale in 200 and 225 °C images.

process has been published in scientific papers. However, its use as a niobium source in ALD has been reported.[18] NiF_2 deposition was studied at 210, 230, and 250 °C. $Ni(thd)_2$ has been reported to decompose at 275 °C,[19] and 250 °C was therefore the highest studied deposition temperature.

According to XRD, all films consist of tetragonal NiF_2 (Fig. 10, ICDD PDF file 24-792). The GPC is 0.67 Å at 210 °C and decreases to 0.53 Å at 250 °C. Films deposited with 1500 cycles using 1 s pulses and purges were measured with ToF-ERDA (Table 2). The F/Ni ratio is 2.0–2.2 and thus in line with the XRD results. The hydrogen and oxygen contents are however large in all films, ranging from 8.3 to 10.7 at%. The carbon content is lower, 2.1–3.7 at%. The Nb content is also modest, 3.9–4.4 at%, with no clear trend with the deposition temperature. In addition, small nitrogen contents (0.03–0.07 at%) were found in the films.

The fast erosion of some ALD metal fluoride films during the ToF-ERDA measurement was observed also with the NiF_2 films. Therefore, no accurate elemental depth profiles were obtained. To investigate if the hydrogen and oxygen impurities are located on the surface and therefore would be due to post-deposition oxidation, one NiF_2 film was capped *in situ* with YF_3 film and measured with ToF-ERDA. YF_3 was deposited at 250 °C by using $Y(thd)_3$ and TaF_5 as precursors. Despite the capping, the hydrogen and oxygen contents are still large indicating that hydrogen and oxygen are probably incorporated into the films already during the deposition. As seen in the depth profiles, hydrogen and oxygen reside clearly in the NiF_2 films (Fig. 11a).

NiF_2 deposition was briefly studied also by using TaF_5 as the fluoride source. The films contained tetragonal NiF_2 as measured by XRD (Fig. 10). One film was capped with YF_3 and measured with ToF-ERDA. The hydrogen and oxygen contents are similar to the films deposited with NbF_5 as the fluoride source. Also in these films hydrogen and oxygen reside clearly in the NiF_2 film as seen in the depth profile (Fig. 11b). The large hydrogen and oxygen contents in the NiF_2 films deposited with both NbF_5 and TaF_5 are assumed to result from the hygroscopicity of the NiF_2 films.

To investigate the differences in the reactivity of $Ni(thd)_2$ towards NH_4F, TiF_4, NbF_5, and TaF_5, thermodynamics were calculated for NiF_2 formation in each case using HSC Chemistry software. There are no thermodynamic data for metal thd complexes and therefore corresponding oxides were used as their approximations. In both thd complexes and metal oxides the metal atoms are bonded to oxygen atoms. The calculations were done in bulk form using the following reaction equations:

$$NiO + 2\ HF\ (g) \rightarrow NiF_2 + H_2O\ (g)$$

$$2\ NiO + TiF_4\ (g) \rightarrow 2\ NiF_2 + TiO_2$$

$$5\ NiO + 2\ NbF_5\ (g) \rightarrow 5\ NiF_2 + Nb_2O_5$$

$$5\ NiO + 2\ TaF_5\ (g) \rightarrow 5\ NiF_2 + Ta_2O_5$$

Table 3 lists the calculated Gibbs free energies for the formation of one mole of NiF_2 at 250 °C. The successful fluoride precursors NbF_5 and TaF_5 have the most thermodynamically

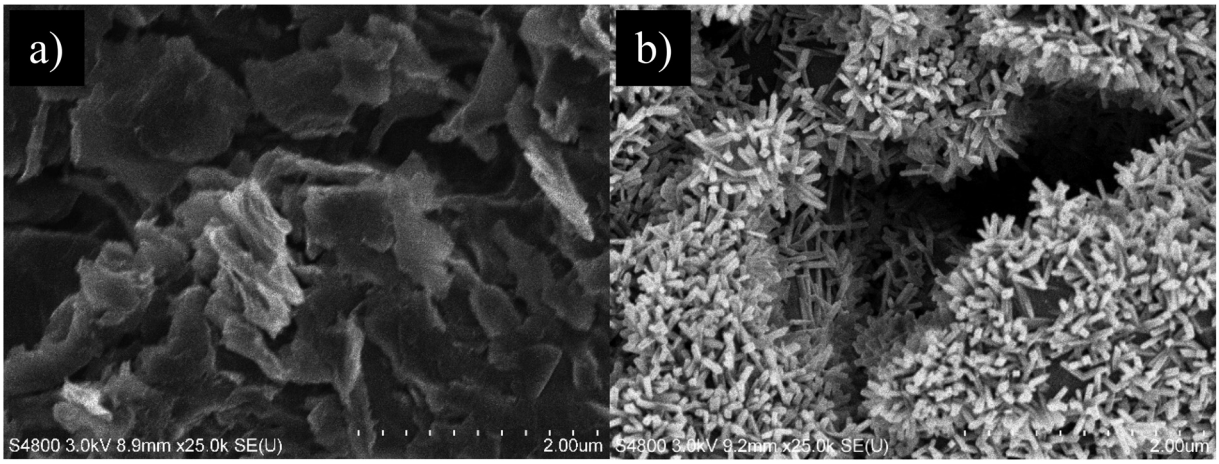

Fig. 8 FESEM images of (a) the bare graphite substrate and (b) a CoF_2 film deposited on the graphite substrate.

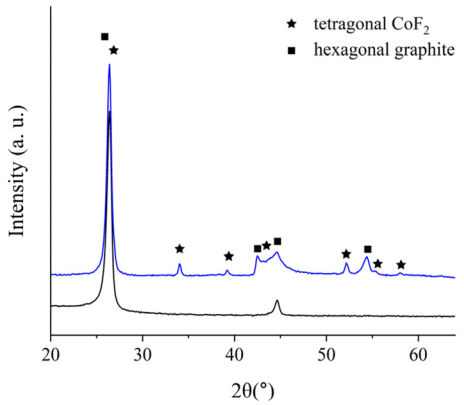

Fig. 9 GI-XRD of a bare graphite substrate and a CoF_2 film deposited at 250 °C on a graphite substrate.

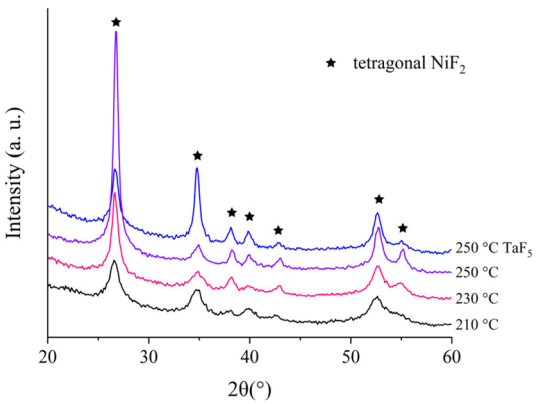

Fig. 10 GI-XRD of NiF_2 films deposited with NbF_5 and TaF_5 as precursors.

favorable reactions, but there are no noteworthy differences in the Gibbs free energies, especially between TiF_4 and NbF_5. The reason for obtaining film growth with NbF_5 but not with TiF_4 is thus not likely explained by thermodynamics alone.

Similar calculations were done also for the formation of one mole of CoF_2 at 250 °C from $Co(thd)_2$ and NH_4F, TiF_4, NbF_5, or TaF_5 using metal oxides as approximations for metal thd complexes (Table 3). Also in this case NbF_5 and TaF_5 have the most thermodynamically favorable reactions, but there are no large differences in the Gibbs free energies.

Thermodynamics were calculated also for the reactions $NiCl_2$ + 2 HF (g) → NiF_2 + 2 HCl (g) and $CoCl_2$ + 2 HF (g) → CoF_2 + 2 HCl (g). The Gibbs free energy for the formation of one mole of NiF_2 at 250 °C is 9.5 kJ whereas for CoF_2 it is 2.6 kJ. There is thus no large difference in the favorability of the reactions, although the combination of $CoCl_2$(TMEDA) + NH_4F resulted in CoF_2 growth and the combination of $NiCl_2$(TMPDA) + NH_4F did not result in NiF_2 growth.

Note that the Gibbs free energy for the CoF_2 formation is positive for the successful combination of $CoCl_2$ and NH_4F whereas it is negative for the combinations of $Co(thd)_2$ and NH_4F, TiF_4, NbF_5, or TaF_5. In the calculations the metal thd complexes have been approximated as metal oxides and in the case of $CoCl_2$(TMEDA) and $NiCl_2$(TMPDA) the reacting species is thought to be $CoCl_2$ and $NiCl_2$. Due to these approximations and assumptions the calculations should be used only to roughly compare the favorability of CoF_2 and NiF_2 formation from similar precursor combinations. Mechanistical studies would be needed to get more insight on the differences in the growth behavior of NiF_2 and CoF_2. These studies are however out of the scope of this study.

Holmium fluoride films

Despite the impurity contents in NiF_2 films, NbF_5 seemed to be a potential fluoride source, especially because the use of TiF_4 and NH_4F as fluoride sources did not produce any film. To show that NbF_5 is usable in ALD, we investigated deposition of another metal fluoride—HoF_3—by using NbF_5 as the fluoride source and $Ho(thd)_3$ as the holmium source. We chose a rare earth ion since they are known to form fluorides easily. Of the rare earth fluorides an ALD process has been reported for

Table 2 Elemental contents and stoichiometry of NiF_2 films (F/Ni ratio 2.0–2.2) deposited with 1500 cycles at different deposition temperatures as measured by ToF-ERDA

T_{dep} (°C)	Ni (at%)	F (at%)	H (at%)	C (at%)	N (at%)	O (at%)	Nb (at%)	F/Ni
210	24.8 ± 0.5	49 ± 2	10 ± 2	3.7 ± 0.8	0.03 ± 0.01	8.3 ± 0.8	4.0 ± 0.2	2.0
230	22.8 ± 0.5	51 ± 2	9.7 ± 1.2	3.0 ± 0.8	0.07 ± 0.01	9.6 ± 0.7	3.9 ± 0.1	2.2
250	23.5 ± 0.6	50 ± 3	10 ± 2	2.1 ± 0.6	0.04 ± 0.01	10.7 ± 0.9	4.4 ± 0.2	2.1

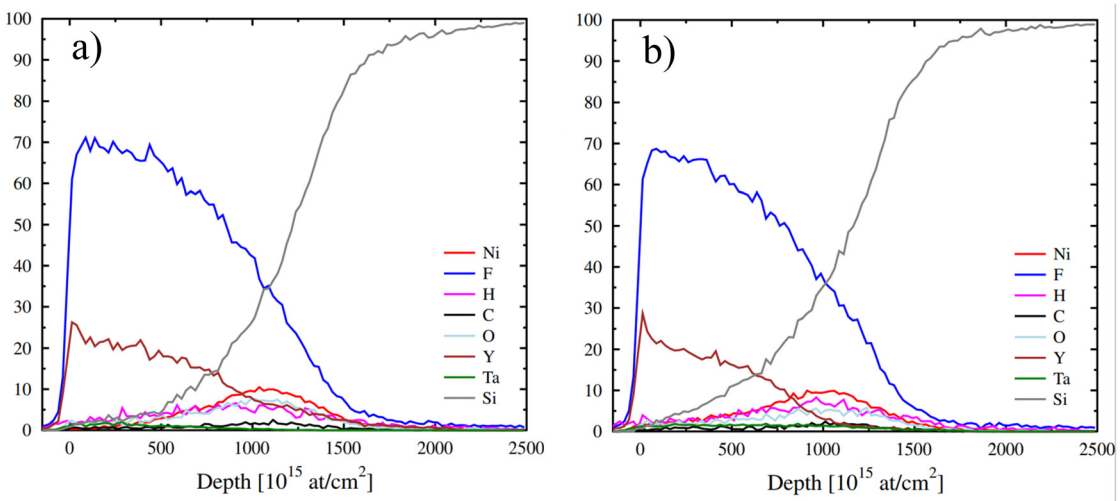

Fig. 11 Elemental depth profiles of YF_3-capped NiF_2 films deposited using (a) NbF_5 or (b) TaF_5 as fluoride source as measured by ToF-ERDA.

Table 3 Calculated Gibbs free energies for the formation of one mole of NiF_2 and CoF_2 at 250 °C from different precursors. NiO and CoO serve as approximations for $Ni(thd)_2$ and $Co(thd)_2$

Metal source	Fluoride source	ΔG (kJ mol^{-1})
NiO	HF (from NH_4F)	−48
NiO	TiF_4	−64
NiO	NbF_5	−67
NiO	TaF_5	−76
CoO	HF (from NH_4F)	−62
CoO	TiF_4	−78
CoO	NbF_5	−82
CoO	TaF_5	−90

YF_3, LaF_3, and TbF_3 using metal thd and TiF_4 as precursors[20–22] and for SmF_3, EuF_3, GdF_3, and TbF_3 using metal thd and NH_4F as precursors.[23,24] We chose HoF_3, a potential material for laser applications,[25] since it has not been deposited earlier by ALD. It is likely that NbF_5 is usable also in the deposition of other rare earth fluorides due to the similar nature of the rare earth metals.

The deposition was studied at 200–275 °C. Orthorhombic HoF_3 was obtained at all deposition temperatures as measured by XRD (Fig. 12, ICDD PDF 23-284). Saturation of the growth per cycle with respect to pulse lengths was verified at 250 °C (Fig. 13). The $Ho(thd)_3$ pulse was varied between 1 and 3.5 s while keeping the NbF_5 pulses at 2 s and purges at 2 s. The GPC saturates around 2 s $Ho(thd)_3$ pulses to ~1 Å (Fig. 13a). The NbF_5 pulse length was varied between 0.5 and 3 s while

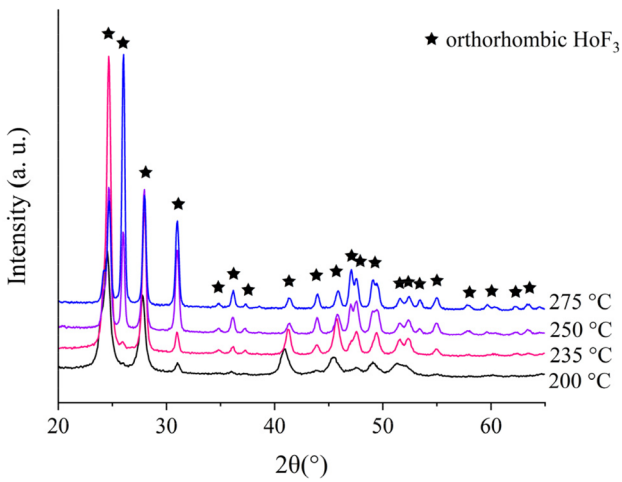

Fig. 12 GI-XRD of HoF_3 films deposited at 200–275 °C.

keeping the $Ho(thd)_3$ pulses at 3 s and purges at 2 s. Saturation of GPC is achieved with 1 s NbF_5 pulses (Fig. 13b).

The stoichiometry and elemental contents in the films were measured with ToF-ERDA (Table 4). The F/Ho ratio varies between 2.9 and 3.4 with no clear deposition temperature dependence. The ratio is in line with the XRD results. In the film deposited at 200 °C the impurity contents are quite large. The hydrogen content is the highest, 11.2 at%, followed by the oxygen content (8.1 at%). The Nb content is however modest,

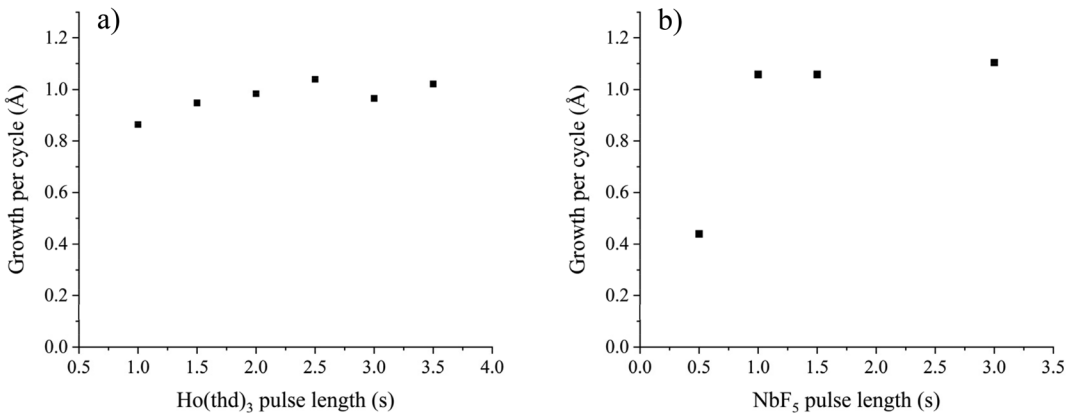

Fig. 13 GPC as a function of (a) $Ho(thd)_3$ and (b) NbF_5 pulse lengths at 250 °C.

Table 4 Elemental contents and stoichiometry of 84–97 nm HoF_3 films (F/Ho ratio 2.9–3.4) deposited at different deposition temperatures as measured by ToF-ERDA

T_{dep} (°C)	Ho (at%)	F (at%)	H (at%)	C (at%)	N (at%)	O (at%)	Nb (at%)	F/Ho
200	19.2 ± 0.2	55.5 ± 1.2	11.2 ± 1.1	3.7 ± 0.4	<0.03	8.1 ± 0.5	2.3 ± 0.2	2.9
235	20.5 ± 0.2	69.9 ± 1.3	4.3 ± 0.6	1.2 ± 0.2	<0.07	2.9 ± 0.2	1.24 ± 0.12	3.4
250	23.4 ± 0.2	73.4 ± 1.5	1.1 ± 0.3	0.43 ± 0.09	<0.03	1.5 ± 0.2	0.21 ± 0.04	3.1
275	22.8 ± 0.2	74.4 ± 1.5	0.7 ± 0.2	0.30 ± 0.09	<0.05	1.6 ± 0.2	0.15 ± 0.03	3.3

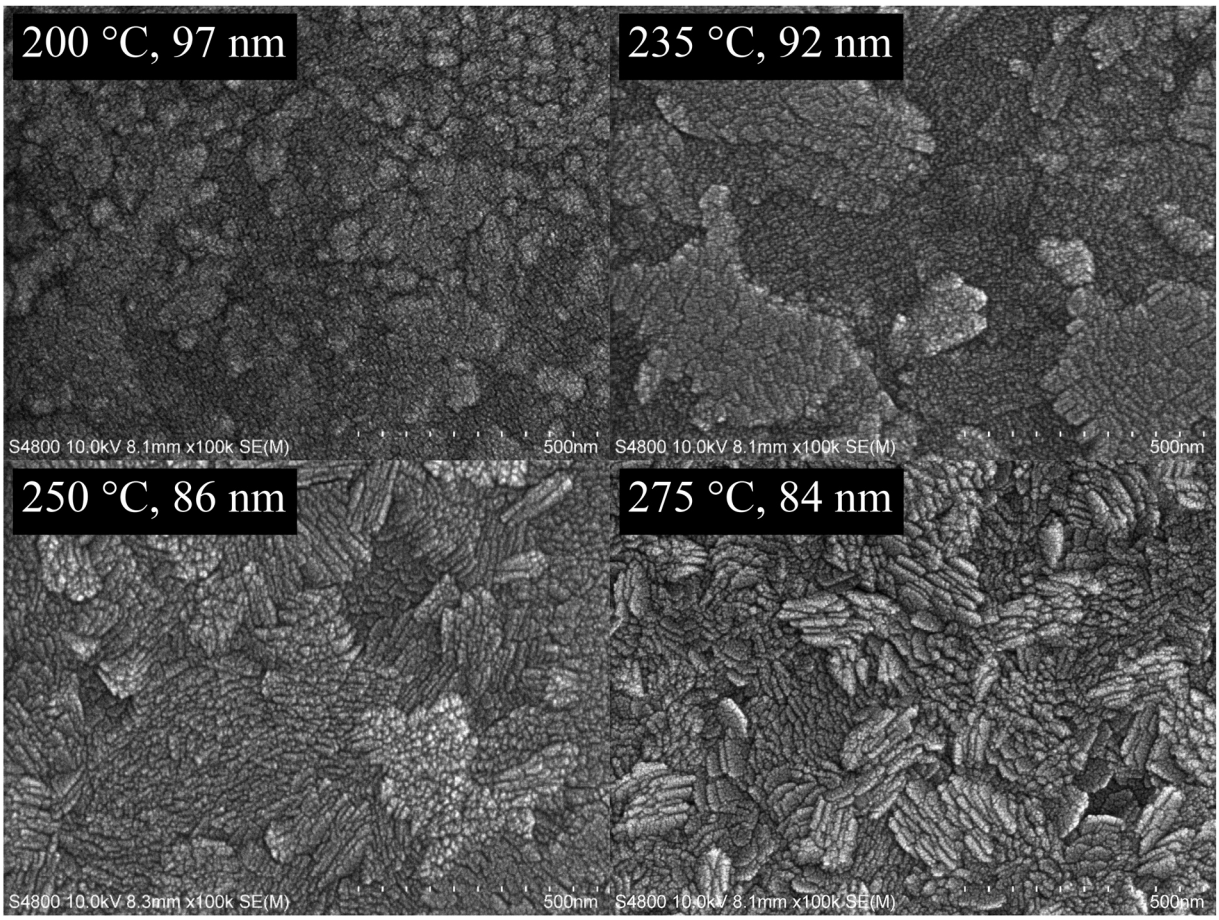

Fig. 14 FESEM images of HoF_3 films deposited at 200–275 °C.

2.3 at%. The films deposited at 235–275 °C are purer, especially the films deposited at 250 and 275 °C. The main impurity in both films is oxygen (1.5 and 1.6 at%). Importantly, the Nb contents are only 0.21 and 0.15 at%.

In FESEM, the 84–97 nm thick films show a lamellar structure, best seen at higher deposition temperatures (Fig. 14). Similar morphology was observed in YF_3 films deposited with ALD.[20] The film deposited at 200 °C looks smoother, but the impurity content is also larger than in the other films.

Conclusions

An ALD process for CoF_2 using $CoCl_2$(TMEDA) and NH_4F as precursors was developed. Depositions at 180–275 °C result in tetragonal CoF_2. The composition of the film is close to stoichiometric, and the H, C, N, O, and Cl impurities are low as measured by ToF-ERDA. As an example, the total impurity content of these impurities in a CoF_2 film deposited at 250 °C is only 1.15 at%. The films grow in rod-like morphology at lower deposition temperatures, whereas at higher deposition temperatures the films are smoother as seen in both SEM and cross-section SEM. Due to the morphology, the films deposited at low temperatures are very rough, *e.g.*, rms roughness is 24.7 nm for a 69 nm film. CoF_2 growth on graphite was also briefly studied at a deposition temperature of 250 °C. Tetragonal CoF_2 with a rod-like morphology was obtained. CoF_2 deposition was also attempted with the precursor combinations of $Co(thd)_2$ and NH_4F, TiF_4, TaF_5, or NbF_5. Either no film growth was seen or there was substantial metal impurity incorporation in the CoF_2 films.

NiF_2 deposition was studied by using the precursor combinations of $Ni(thd)_2$ + NH_4F, TiF_4, TaF_5, or NbF_5 and $NiCl_2$(TMPDA) + NH_4F which is similar to the precursor combination found successful for the CoF_2 deposition. Film growth was observed only when $Ni(thd)_2$ was combined with NbF_5 or TaF_5. The films deposited at 210–250 °C by using NbF_5 are tetragonal NiF_2 according to XRD. However, the films have large hydrogen and oxygen contents as measured by ToF-ERDA. The H and O contents were large in the NiF_2 films also when the films were *in situ* capped with YF_3, indicating their incorporation into the films already during the deposition. Similar H and O contents were seen also when TaF_5 was used as the fluoride source.

The most remarkable difference between CoF_2 and NiF_2 is the hygroscopicity of NiF_2. In addition, $CoCl_2$(TMEDA) and NH_4F resulted in film growth whereas the combination of $NiCl_2$(TMPDA) and NH_4F did not produce any film. There are however no large differences in the Gibbs free energy of the formation of CoF_2 and NiF_2 from these precursors. With both cobalt and nickel the favorability of the reaction between the metal thd (approximated in calculations as oxides) and a different fluoride source increases in the order NH_4F – TiF_4–NbF_5–TaF_5. There are no large differences in the Gibbs free energies, however. CoF_2 formation is in general slightly more favorable than NiF_2 formation. In both cases no film was obtained with NH_4F as the fluoride source. In the case of cobalt, a film was obtained with TiF_4, NbF_5 and TaF_5, but severe metal impurity incorporation was seen. In the case of nickel, film was obtained only with NbF_5 or TaF_5 as the fluoride source. Reaction mechanism studies could reveal the differences in the growth of CoF_2 and NiF_2, but those are out of the scope of the current paper.

Since NbF_5 is a new fluoride source in ALD, we wanted to show that it can be used to deposit good quality ALD metal fluoride films. Thus, we studied the deposition of HoF_3 by combining NbF_5 with $Ho(thd)_3$. Orthorhombic HoF_3 films were obtained at all the studied deposition temperatures 200–275 °C. The saturation of the GPC with respect to both precursor pulses was achieved at 250 °C. The films deposited at 235–275 °C are pure according to ToF-ERDA, *e.g.*, in the films deposited at 250 and 275 °C the Nb contents are only 0.21 and 0.15 at%. In addition to producing pure HoF_3 films, NbF_5 produced films with $Ni(thd)_2$ when no growth was observed with TiF_4 or NH_4F. NbF_5 is thus a potential fluoride source in ALD.

Conflicts of interest

There are no conflicts of interest to declare.

Acknowledgements

The use of ALD Center Finland research infrastructure is acknowledged. Johanna Majlund is acknowledged for performing some of the depositions.

References

1 K. Lemoine, A. Hémon-Ribaud, M. Leblanc, J. Lhoste, J.-M. Tarascon and V. Maisonneuve, *Chem. Rev.*, 2022, **122**, 14405–14439.
2 Z.-W. Fu, C.-L. Li, W.-Y. Liu, J. Ma, Y. Wang and Q.-Z. Qin, *J. Electrochem. Soc.*, 2005, **152**, E50.
3 D. Streblechenko and M. R. Scheinfein, *J. Vac. Sci. Technol., A*, 1998, **16**, 1374–1379.
4 M. Malac, M. Schoefield, Y. Zhu and R. Egerton, *J. Appl. Phys.*, 2002, **92**, 1112–1121.
5 P. A. Young, *Thin Solid Films*, 1969, **4**, 25–33.
6 D. Lederman, D. P. Belanger, J. Wang, S.-J. Han, C. Paduani, C. A. Ramos and R. M. Nicklow, *MRS Online Proc. Libr.*, 1993, **313**, 333–338.
7 M. Leskelä and M. Ritala, *Angew. Chem., Int. Ed.*, 2003, **42**, 5548–5554.
8 X. Meng, X.-Q. Yang and X. Sun, *Adv. Mater.*, 2012, **24**, 3589–3615.
9 M. Mäntymäki, J. Hämäläinen, E. Puukilainen, F. Munnik, M. Ritala and M. Leskelä, *Chem. Vap. Deposition*, 2013, **19**, 111–116.

10 Y. Lee, J. W. DuMont, A. S. Cavanagh and S. M. George, *J. Phys. Chem. C*, 2015, **119**, 14185–14194.
11 K. Väyrynen, T. Hatanpää, M. Mattinen, M. Heikkilä, K. Mizohata, K. Meinander, J. Räisänen, M. Ritala and M. Leskelä, *Chem. Mater.*, 2018, **30**, 3499–3507.
12 K. Väyrynen, T. Hatanpää, M. Mattinen, K. Mizohata, K. Meinander, J. Räisänen, J. Link, R. Stern, M. Ritala and M. Leskelä, *Adv. Mater. Interfaces*, 2019, **6**, 1801291.
13 M. Ylilammi and T. Ranta-aho, *J. Electrochem. Soc.*, 1994, **141**, 1278–1284.
14 M. Mäntymäki, M. J. Heikkilä, E. Puukilainen, K. Mizohata, B. Marchand, J. Räisänen, M. Ritala and M. Leskelä, *Chem. Mater.*, 2015, **27**, 604–611.
15 M. Anji Reddy, B. Breitung, V. S. K. Chakravadhanula, C. Wall, M. Engel, C. Kübel, A. K. Powell, H. Hahn and M. Fichtner, *Adv. Energy Mater.*, 2013, **3**, 308–313.
16 J. W. Elam, A. U. Mane and M. Gebhard, US20210254209A1, p. 2021.
17 M. Mäntymäki, M. Ritala and M. Leskelä, US9394609B2, 2016.
18 T. Proslier, J. A. Klug, J. W. Elam, H. Claus, N. G. Becker and M. J. Pellin, *J. Phys. Chem. C*, 2011, **115**, 9477–9485.
19 E. Lindahl, M. Ottosson and J.-O. Carlsson, *Chem. Vap. Deposition*, 2009, **15**, 186–191.
20 T. Pilvi, E. Puukilainen, F. Munnik, M. Leskelä and M. Ritala, *Chem. Vap. Deposition*, 2009, **15**, 27–32.
21 T. Pilvi, E. Puukilainen, K. Arstila, M. Leskelä and M. Ritala, *Chem. Vap. Deposition*, 2008, **14**, 85–91.
22 E. Atosuo, J. Ojala, M. J. Heikkilä, M. Mattinen, K. Mizohata, J. Räisänen, M. Leskelä and M. Ritala, *J. Vac. Sci. Technol., A*, 2021, **39**(2), 022404.
23 P.-A. Hansen, T. Zikmund, T. Yu, J. Nitsche Kvalvik, T. Aarholt, Ø. Prytz, A. Meijerink and O. Nilsen, *Commun. Chem.*, 2020, **3**, 162.
24 E. Atosuo, K. Mizohata, M. Mattinen, M. Mäntymäki, M. Vehkamäki, M. Leskelä and M. Ritala, *J. Vac. Sci. Technol., A*, 2022, **40**(2), 022402.
25 F. Jobin, P. Paradis, Y. Ozan Aydin, T. Boilard, V. Fortin, J.-C. Gauthier, M. Lemieux-Tanguay, S. Magnan-Saucier, L.-C. Michaud, S. Mondor, L.-P. Pleau, L. Talbot, M. Bernier and R. Vallée, *Opt. Express*, 2022, **30**, 8615–8640.